Customized High-Sensitivity Plasmonic Metasensing Towards Immunodetection of Single Bio-Nanoparticles

Jiaqing Shen, Fajun Li, Zhenbiao Wang, Xueying Liu, Yinong Xie, Wei Chen, Ming Hui Fang, and Jinfeng Zhu, *Senior Member, IEEE*

***Abstract*—Plasmonic metasurface biosensing has shown great potential in label-free detection of bio-nanoparticles with various sizes, such as cancer antigens, exosomes and SARS-CoV-2 virus. It typically relies on the immunoassay, but current studies usually neglect the perfect size matching between each target bio-nanoparticle and the surface near-field domain, which should be very critical for the enhancement of detection performance. In order to maximize the immunodetection capability for each bio-nanoparticle, we propose a plasmonic meta-biosensor based on the field-customized mechanism. Our design overcomes the serious interference of biofunctionalization and accomplishes a sensitivity of 27 times higher than the conventional nanoplasmonic counterpart. Our method also builds the important basis of single bio-nanoparticle immunodetection by a plasmonic metasurface. The customized plasmonic metasensing study implies a promising way towards ultra-low concentration biosensing or even single bio-nanoparticle detection for high-performance point-of-care-testing in the near future.**

***Index Terms*—Plasmonics, customized, immunodetection, meta-biosensors.**

I. Introduction

PLASMONIC metasurfaces have extraordinary optical properties and hold great promise in biomarker sensing, particularly for point-of-care-testing (POCT) [1], [2], [3], [4], [5]. Typically, plasmonic metasurface biosensors are based on the local refractive index sensing above periodic metaunit cells consisting of metal or metal/dielectric (M/D) nanostructures, which support high optical field confinement and enhancement induced by surface plasmons [6], [7], [8], [9]. The identification and concentration measurement of target bio-nanoparticles (TBNs) usually rely on the specific binding on the biorecognition elements (BEs) of the meta-biosensors (e.g. meta-biosensors based on immunoassay). In general, the most sensitive surface region is limited within the evanescent decay length above the plasmonic metasurfaces, but they typically require biofunctionalization in order to bind TBNs beforehand, which inevitably occupies the region with the strongest optical field [10], [11], [12], [13], [14], and severely lowers the space utilization of optical near field induced by plasmonic effects. Moreover, the sizes of TBNs to be detected are usually diversified, such as cancer antigens with the characteristic scale of 10–40 nm [15], [16], [17], and exosomes and SARS-CoV-2 virus with the sizes of 50–150 nm [18], [19]. Significant efforts have been made on optimizing the sensitivity of binding TBNs by enhancing the local field intensity with metal nanostructures of various shapes, such as nanohole, nanocup, nanonail and so on [20], [21], [22], [23], [24], [25], [26], [27], [28]. Despite these efforts, the size matching between the space near field and TBNs remains a significant issue. Therefore, a TBN-customized plasmonic metasurface sensor with high space near-field utilization is still quite in demand for highly-sensitive detection of biospecificity.

In this work, we propose a kind of plasmonic meta-biosensors with TBN-customized void M/D nanocylinder metaunits for high-sensitivity immunodetection. Our approach demonstrates much higher TBN sensitivity than conventional metasurface sensing and implies a great potential towards nanoplasmonic digital immunoassay by a TBN-customized metasensing scheme. The sensing mechanism is systematically illuminated by the theoretical analysis and full-wave simulation. One can detect each kind of TBN with an optimized high sensitivity by engineering the M/D hybrid metastructure. Our metasensing study provides an important guide for developing nanoplasmonic digital immunoassay, which implies a promising potential in future POCT applications.

Manuscript received 19 April 2022; revised 2 November 2022; accepted 6 January 2023. Date of publication 10 January 2023; date of current version 19 January 2023. This work was supported in part by the National Natural Science Foundation of China under Grant 62175205, in part by the Natural Science Foundation of Fujian Province under Grant 2020J06009, and in part by the National Safety Academy Foundation under Grants U2130112 and U1830116. *(Corresponding author: Jinfeng Zhu.)*

Jiaqing Shen, Fajun Li, Zhenbiao Wang, Xueying Liu, Yinong Xie, Wei Chen, and Ming Hui Fang are with the Institute of Electromagnetics and Acoustics and Key Laboratory of Electromagnetic Wave Science and Detection Technology, Xiamen University, Xiamen 361005, China (e-mail: 34320210155961@stu.xmu.edu.cn; 18251950300@163.com; 34320201150180@stu.xmu.edu.cn; 34320190153851@stu.xmu.edu.cn; m18724727110@163.com; nanooptics@stu.xmu.edu.cn; seanfang05080326@163.com).

Jinfeng Zhu is with the Institute of Electromagnetics and Acoustics and Key Laboratory of Electromagnetic Wave Science and Detection Technology, Xiamen University, Xiamen 361005, China, and also with the State Key Laboratory of Applied Optics, Changchun Institute of Optics, Fine Mechanics and Physics, Chinese Academy of Sciences, Changchun 130033, China (e-mail: nanoantenna@hotmail.com).

Color versions of one or more figures in this article are available at https://doi.org/10.1109/JSTQE.2023.3235723.

Digital Object Identifier 10.1109/JSTQE.2023.3235723

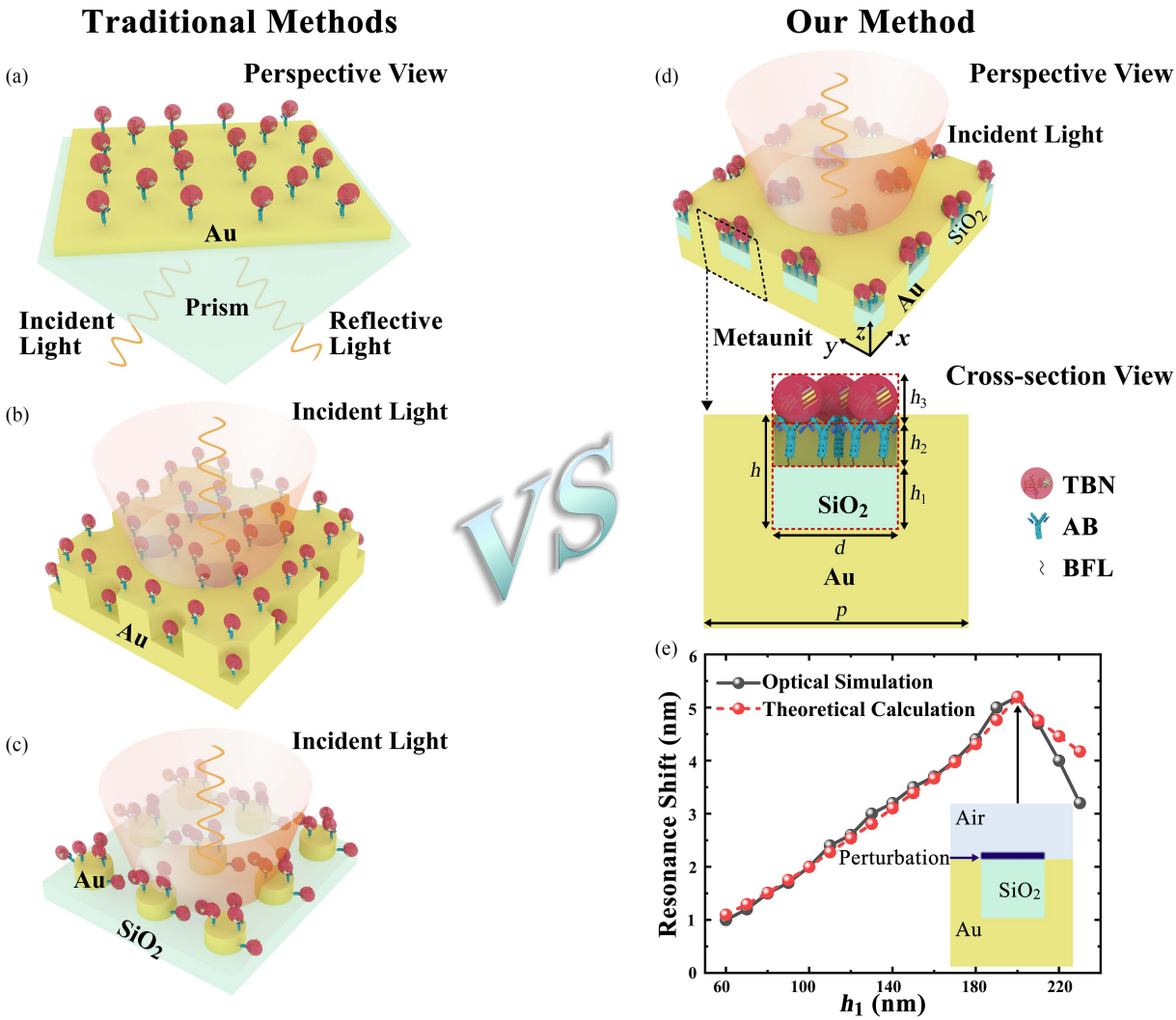

Fig. 1. (a), (b), and (c) are the schematic drawings of traditional biosensing methods based on PSPR, GSPP and LSPR, respectively. (d) Perspective and cross-section views for the illustration of M/D hybrid meta-biosensor, where p, d, h, h_1, h_2 and h_3 represent the period of metaunit, the diameter of void gold nanocylinders, the heights of void gold nanocylinders, SiO_2 nanocylinders, BEs and TBNs, respectively. (e) Plasmonic resonance shift $\Delta\lambda$ as a function of perturbation position h_1.

II. Design and Method

The traditional biosensing methods of prism-based surface plasmon resonance (PSPR), 2D grating surface plasmon polarizations (GSPP) and localized surface plasmon resonance (LSPR) are compared with our meta-biosensing approach in Fig. 1. Particularly, the M/D hybrid metasurface for TBN-customized sensing is illustrated in Fig. 1(d). The M/D hybrid metasurface can be fabricated by a series of nanotechnology processes, including nanoimprint lithography, plasma etching, and electron beam evaporation [29], [30]. It consists of an array of periodic subwavelength void gold nanocylinders, each of which is partially filled with silicon dioxide (SiO_2). The metasurface acts as a two-dimensional array with orthogonal reciprocal lattice vectors, which allows for the nanograting-coupled plasmonic mode and traps the spatial light wave around the wavelength of plasmonic resonance [31]. The metasurface works in the visible regime, and the material optical parameters of SiO_2 are obtained from Reference [32]. We adopt the immunoassay scheme for the meta-biosensor by using the specific binding between the BE and TBN [33]. BE consists of biological functional layer (BFL) and antibody (AB). In each metaunit, the biorecognition element is specifically immobilized on top of the SiO_2 component [34], and it can capture the TBN in the process of immunodetection. The optical simulation based on the finite element method (Comsol Multiphysics) is used to investigate the sensing mechanism and optimize the detection performance. In the simulation, all the materials are assumed to be isotropic, and the Floquet boundary conditions are applied for the periodic unit cells. The size of z-direction unit cell in simulation is the same as the x-direction (i.e., 480 nm). Two perfect matching layers with the thickness of 500 nm are located in the appropriate position on the top and the bottom of the unit cell, respectively. The s-polarized wave is applied as the incident light. Adaptive inhomogeneous tetrahedral mesh is adopted to discretize the metaunits, and the minimum edge length of the mesh element is as small as 0.5 nm to ensure the convergence and reproducibility of the simulation.

In order to demonstrate the physics, we first study the 5 nm thick SiO_2 perturbation response on the metastructure without biological components in Fig. 1(e). The shift of spectral resonance wavelength as a function of introducing a 5 nm perturbation for a series of SiO_2 thickness h_1. As h_1 increases from 60 nm to 200 nm, $\Delta\lambda$ progressively rises and approaches a maximum of 5.2 nm, and it gradually drops down for h_1 changing from 200 nm to 230 nm. This result can be explained by the perturbation theory, which derives explicit formulas for the resonance shift of plasmonic metasurface. The analytical solution of the electric field and resonance wavenumber for the fundamental plasmonic mode can be expressed as below [35],

$$\frac{1}{\mu\varepsilon}\nabla^2 E = -(ck)^2 E \tag{1}$$

where μ and ε represent the environmental permeability and permittivity surrounding the plasmonic metasurface, respectively. k, c and E denote the plasmonic wavenumber, speed of light and electric field, respectively. Here we take Ω instead of $\frac{1}{\mu\varepsilon}\nabla^2$, whose eigenvalue is -$(ck)^2$. When the perturbative medium (permittivity ε_p, permeability μ) with the volume of V_p is introduced into the plasmonic metasurface, the wavenumber and electric field on the plasmonic metasurface would have a slight change. In the volume of V_p, Ω can be ex-pressed as below,

$$\begin{aligned}\Omega &= \frac{1}{\mu\varepsilon_p}\nabla^2 = \frac{1}{\mu\varepsilon_0}\nabla^2 + \left(\frac{\mu\varepsilon_0}{\mu\varepsilon_p} - 1\right)\frac{1}{\mu\varepsilon_0}\nabla^2 \\ &= \Omega_0 + \left(\frac{\varepsilon_0}{\varepsilon_p} - 1\right)\Omega_0 = \Omega_0 + \Omega_1\end{aligned} \tag{2}$$

where $\Omega_0 = \frac{1}{\mu\varepsilon_0}\nabla^2$, $\Omega_1 = (\frac{\varepsilon_0}{\varepsilon_p} - 1)\Omega_0$ and ε_0 is the environmental permittivity without the perturbation. In the environmental region outside V_p, Ω_1 equals to 0. The changed electric field can be expanded in a series as below,

$$E = \sum_n a_n E_n \ (a_0 = 1, n = 0, 1, 2, 3\ldots) \tag{3}$$

After introducing the perturbation, we take the first-order electric field approximation for (2), combine it with (1), and have the following equation,

$$\begin{aligned}&k_0^2 E_0 + k_0^2 a_1 E_1 + \left(\frac{\varepsilon_0}{\varepsilon_p} - 1\right)k_0^2 E_0 + \left(\frac{\varepsilon_0}{\varepsilon_p} - 1\right)k_0^2 a_1 E_1 \\ &\quad = k_1^2 E_0 + k_1^2 a_1 E_1\end{aligned} \tag{4}$$

The above equation is scalarly multiplied by E_0^* (the conjugate of E_0) and integrated throughout the environmental volume V_{nf} for plasmonic near-field sensing region, and we have the expression of first-order wavenumber as below,

$$k_1^2 = k_0^2 + k_0^2\left(\frac{\varepsilon_0}{\varepsilon_p} - 1\right)\frac{\int_{V_p}|E_0|^2 dV_p}{\int_{V_{nf}}|E_0|^2 dV_{nf}} \tag{5}$$

Equation (5) can be changed into the following expression,

$$\frac{\Delta k}{k_0} \approx \left(\frac{\varepsilon_e}{\varepsilon_p} - 1\right)\frac{\int_{V_p}|E_0|^2 dV_p}{2\int_{V_{nf}}|E_0|^2 dV_{nf}} \tag{6}$$

where $\Delta k = k_1 - k_0$ and $k_1 + k_0 \approx 2k_0$. Therefore, the wavelength shift of plasmonic resonance can be expressed as below,

$$\Delta\lambda \approx \frac{\lambda_1}{2}\frac{\Delta\varepsilon\int_{V_p}|E_0|^2 dV_p}{\varepsilon_p\int_{V_{nf}}|E_0|^2 dV_{nf}} \tag{7}$$

where $\lambda_1 = 2\pi/k_1$ and $\Delta\varepsilon$ denote the plasmonic resonance wavelength with perturbation and permittivity difference between the perturbation object and environment. As shown in Fig. 1(e), the theoretical calculation based on (7) indicates a good consistency with the full-wave simulation. This demonstrates that the slight changes of SiO_2 thickness inside the gold nanocylinders can lead to obvious spectral shifts of plasmonic resonance wavelengths, especially for $h_1 = h = 200$ nm. The result also implies the high plasmonic sensitivity on dielectric change around the mouth position of the void gold nanocylinder. The above basic analysis would further facilitate our study and understanding for enhancing the optical sensing for introduced TBNs.

III. Results and Discussion

A. TBN-Customized Plasmonic Metasensing

We focus our discussion on the performance of TBN-customized sensors under the immunoassay scheme. To simplify the physical model, we assume the BEs and TBNs as spheres with the fixed diameter of 50 nm, respectively, and compare the sensing performance of traditional and our method by detecting the same amount of TBNs, as shown in Fig. 2. The sensitivity is described as the following equation:

$$S = \frac{\Delta\lambda}{\Delta n \Delta V_{TBN}} \tag{8}$$

where $\Delta n = n_{TBN} - n_e$, ΔV_{TBN}, and $\Delta\lambda$ are the relative change in refractive index, volume of TBNs, and resonance wavelength shift due to the specific binding of TBNs on BEs, respectively. As shown in Fig. 2, for capturing 8 TBNs in the same unit projected area of sensing, traditional methods of PSPR, GSPP, and LSPR correspond to the sensitivities of 6.10×10^{13} $RIU^{-1}m^{-2}$, 0.89×10^{13} $RIU^{-1}m^{-2}$ and 0.24×10^{13} $RIU^{-1}m^{-2}$, respectively. Under the immunodetection mechanism, the sensitivities of traditional metasensing (GSPP and LSPR) for TBNs are even much smaller than the classic PSPR sensing. By introducing the M/D (gold and SiO_2) hybrid metasurfaces as shown in Fig. 2(d) and (e), we can manage to make the sensitivities relatively higher than those of the traditional methods based on GSPP and LSPR (Fig. 2(b) and (c)), but they are still much lower than that of the PSPR configuration. In the M/D hybrid metasurfaces, the TBNs are captured on top of the SiO_2 nanocylinder. As observed in Fig. 2(f), we can further optimize the height of SiO_2 nanocylinder and achieve the maximum TBN sensitivity of 6.48×10^{13} $RIU^{-1}m^{-2}$ at the value of 130 nm. This is much higher than that of the traditional PSPR sensing. The use of 130 nm hight SiO_2 nanocylinder in the M/D hybrid metasurface indicates the best TBN sensitivity, which is about 27 times of that for the traditional LSPR method. These results imply that one can customize or engineer the metaunit structure of M/D hybrid metasurface to pursue a high TBN sensing performance.

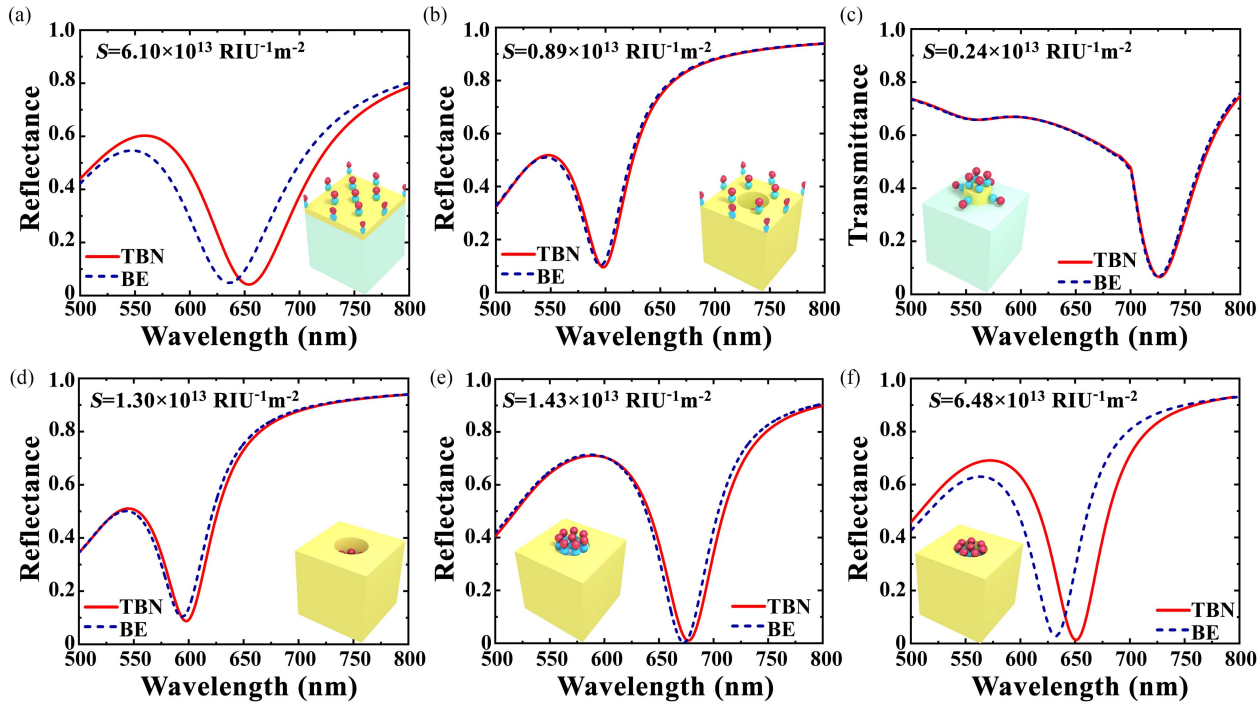

Fig. 2. Reflectance spectra before and after TBN capture: (a) PSPR, where the gold film thickness is 50 nm, and the incident angle is 47°, (b) GSPP, where the void gold nanocylinder diameter and height are 210 nm and 200 nm, respectively, (c) LSPR, where the gold nanocylinder diameter and height are 170 nm and 80 nm, respectively, (d) M/D hybrid metasurface for $h_1 = 30$ nm, (e) M/D hybrid metasurface for $h_1 = 180$ nm, (f) M/D hybrid metasurface for $h_1 = 130$ nm. For all the simulations, $p = 480$ nm, and there are 8 TBNs in each unit cell. For the simulations of (d)-(f), $d = 210$ nm, $h = 200$ nm, and $h_2 = h_3 = 50$ nm.

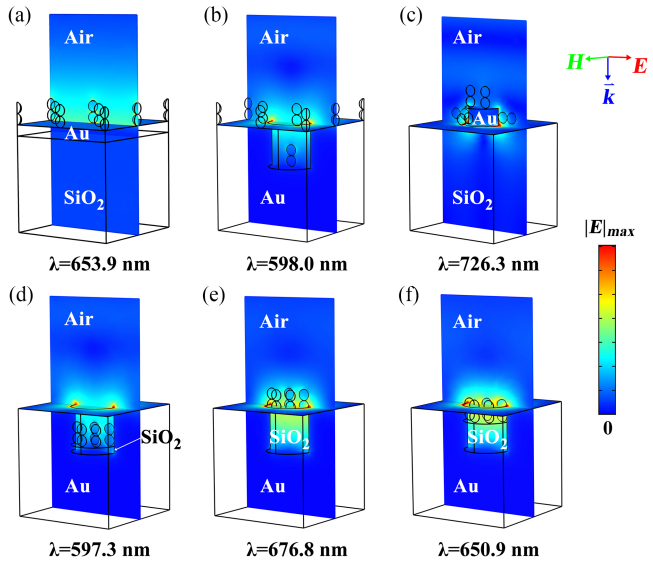

Fig. 3. Field distributions at corresponding resonances for TBN sensing: (a) PSPR, (b) GSPP, (c) LSPR, (d) M/D hybrid metasurface for $h_1 = 30$ nm, (e) M/D hybrid metasurface for $h_1 = 180$ nm, (f) M/D hybrid metasurface for $h_1 = 130$ nm.

In order to reveal the physics of sensitivity enhancement, we further analyze the simulation models through the optical field distributions at resonances, as shown in Fig. 3. In traditional PSPR sensing, the electric field is mainly enhanced on the gold surface, as seen in Fig. 3(a). Due to the use of BE, the TBN will not be located at the region with the strongest electric field. In traditional GSPP sensing, the strongest electric field (namely hot spot) is located at the mouth of void gold nanocylinder, as observed in Fig. 3(b). The random distribution of TBNs makes most of them not located in the region with the strongest electric field. Fig. 3(c) indicates that the strongest electric field is mainly located at the bottom edge of gold nanocylinder for LSPR sensing, while the TBNs are randomly distributed and the hot spots are usually occupied by the BEs. This makes the LSPR sensing performance worse than that of PSPR [36]. In the M/D hybrid metasurface sensing, the highest field intensity is concentrated at the mouth of the void gold nanocylinder, as observed from Fig. 3(d) to (f). For the SiO_2 nanocylinder height $h_1 = 30$ nm, the TBNs are located below the region with the strongest optical field. For $h_1 = 180$ nm, the TBNs are located at the above the hot spot region. In contrast, when the height of SiO_2 nanocylinder is 130 nm, the TBNs are precisely located around the mouth position of void gold nanocylinder, where the light field has the optimal concentration and supports the strongest light-matter interaction. Such effect leads to the significant enhancement of biosensitivity. Therefore, one can customize the height of SiO_2 nanocylinder and maximize the sensitivity for a given kind of TBN by the M/D hybrid metasurface.

B. *Biosensing of TBNs With Various Sizes*

Based on the above analysis, one can design the corresponding optimal biosensing performance for TBNs with various sizes. With the aim to simplify the physical model, the BEs and TBNs are assumed as the equivalent blocks of nanodisks with the

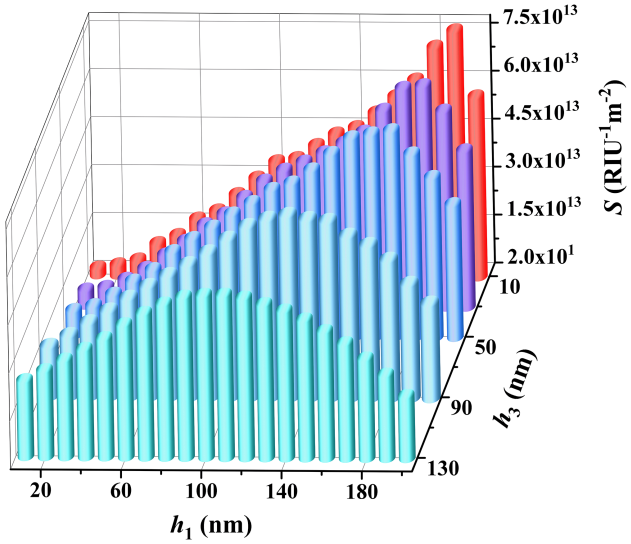

Fig. 4. Optimization of customized meta-biosensor for multiplex TBNs with various sizes, where $p = 480$ nm, $d = 210$ nm, $h = 200$ nm, and $h_2 = 10$ nm.

refractive index of 1.56 [37]. We next optimize the performance of bio-sensors for five kinds of TBNs and the simulated results are shown in Fig. 4. For the specific height of TBNs (e.g. $h_3 = 10$ nm), there is a maximum sensitivity as the h1 changes from 10 nm to 200 nm. The maximum sensitivity for $h_3 = 10$ nm is 7.44×10^{13} RIU^{-1}m^{-2} at $h_1 = 190$ nm. When the height of TBNs increases from 10 nm to 130 nm, the maximum sensitivity for each size gradually reduces from 7.44×10^{13} RIU^{-1}m^{-2} to 5.13×10^{13} RIU^{-1}m^{-2} with the customized optimal h_1 reducing from 190 nm to 110 nm. This result implies that each kind of TBN can have an optimized metastructure for biosensing with the highest sensitivity. One can design the high-performance meta-biosensor according to the size of target biomolecules. It can be observed that for the larger TBNs, such as $h_1 = 130$ nm, the maximum sensitivity is lower than the smaller ones. When the size of TBN is larger than the region of optical field enhancement, the space utilization of near field is less effective. Therefore, one can also optimize the confinement size of space enhanced near field to achieve higher biomolecule-customized sensitivity in the design of meta-biosensor.

C. Single-TBN Biosensing

The mechanism of customized plasmonic metasensing can be also applied on the detection of ultra-low concentration TBNs and even a single TBN (e.g., the exosome or virus [38], [39]. As shown in Fig. 5(a), we plot the shift of resonance wavelength for introducing a single TBN as a function of the diameter d for void gold nanocylinder. As d increases from 150 nm to 210 nm, the TBN sensitivity S gradually drops down from 7.2×10^{13} RIU^{-1}m^{-2} to 2.7×10^{13} RIU^{-1}m^{-2}. This demonstrates that the sensitivity of a TBN highly depends on the diameter of void gold nanocylinder, which can be attributed to the utilization efficiency of near field around the nanocylinder mouth. Particularly, when the diameter of TBN equals to the diameter of void nanocylinder, we can achieve the highest sensitivity. Therefore, one can also

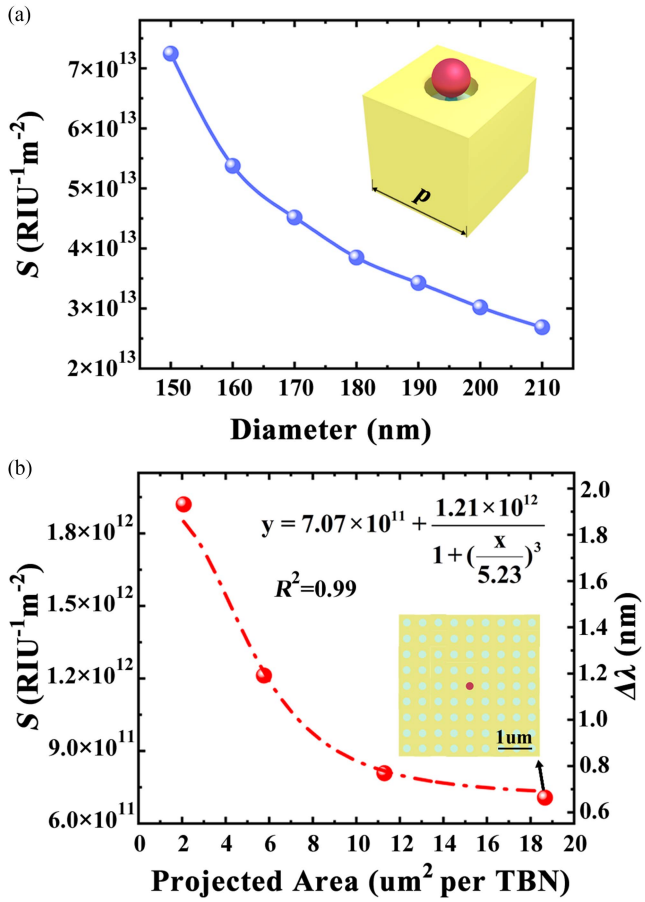

Fig. 5. (a) TBN sensitivity as a function of the diameter of void gold nanocylinder, where the inset denotes the perspective view of a metasurface unit cell, (b) Single-TBN sensitivity as a function of metasurface module area for detecting, where the inset denotes the top view of the metasurface with 9×9 unit cells. For all the simulations, $p = 480$ nm, $h = 200$ nm, $h_1 = 110$ nm, and the diameter of BE and TBN are 10 nm and 150 nm, respectively.

customize the diameter of void gold nanocylinder in the M/D hybrid metasurface according to the size of TBN.

Furthermore, we focus on evaluating the detection sensitivity of a single TBN by using various metasurface module areas, which is a critical criterion for high-precision biosensing of samples with an extremely low concentration. As shown in Fig. 5(b), we plot the sensitivity of a single TBN as a function of the metasurface module area for detecting. With the area increasing from 2.1 um^2 to 18.7 um^2, the spectral sensitivity of a single TBN gradually drops from 1.9×10^{12} RIU^{-1}m^{-2} to 7.0×10^{11} RIU^{-1}m^{-2}. The simulated data points are well fitted with the four-parameter logistic curve with a correlation coefficient R^2 of 0.99 [40]. In combination with a series of metasurface modules, hyperspectral measurement can be applied to the detection of a single TBN in a biochip [41]. For a commercial hyperspectral measuring system, the spectrometer resolution and signal-to-noise ratio in the visible range can be as low 0.07 nm and 2000/1, respectively [42]. When we apply a sufficient metasurface module area of 18.7 um^2 for detecting a single TBN, the spectral shift of resonance wavelength is 0.7 nm, which is 10 times of the smallest spectral resolution. Such

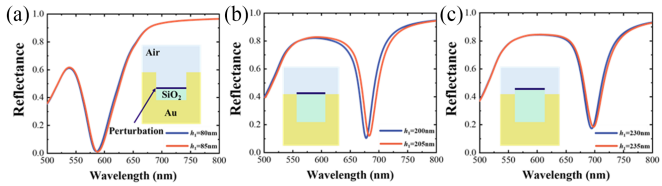

Fig. 6. (a), (b), and (c) are the reflection spectra of M/D hybrid metastructure for perturbation position h_1 with the values of 80 nm, 200 nm, and 230 nm, respectively.

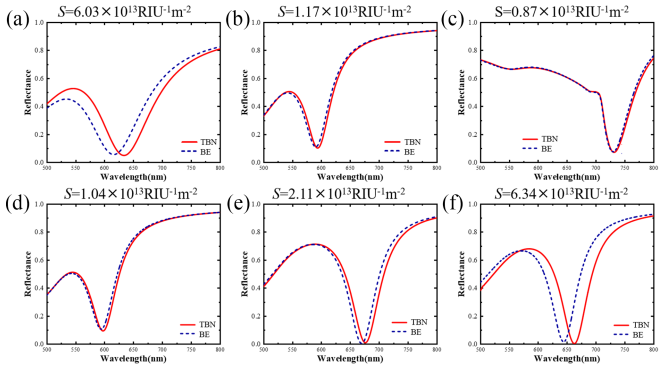

Fig. 7. Reflectance spectra before and after TBN capture: (a) PSPR, where the gold film thickness is 50 nm, and the incident angle is 47°, (b) GSPP, where the void gold nanocylinder diameter and height are 210 nm and 200 nm, respectively, (c) LSPR, where the gold nanocylinder diameter and height are 170 nm and 80 nm, respectively, (d) M/D hybrid metasurface for $h_1 = 30$ nm, (e) M/D hybrid metasurface for $h_1 = 180$ nm, (f) M/D hybrid metasurface for $h_1 = 130$ nm. For all the simulations, $p = 480$ nm, and there are 8 TBNs in each unit cell. For the simulations of (d)-(f), $d = 210$ nm, $h = 200$ nm, $h_2 = 20$ nm, and $h_3 = 50$ nm.

sensing capability indicates that one can capture the single-TBN signal effectively by using a hyperspectral sensing over a series of metasurface modules on a biochip. Therefore, the pro-posed customized plasmonic metasensing would be very promising for the future studies of single-TBN immunodetection in a non-invasive and label-free manner.

IV. Conclusion

In summary, we propose the immunosensing scheme of M/D hybrid plasmonic meta-biosensor by engineering the surface location of various TBNs. By tuning the size of dielectric components in the metaunits, the utilization of space near field is maximized, which leads to very high immunodetection sensitivity. The sensor is also universal to enhance the detection capability for many kinds of TBNs by a metasurface-customized approach. Furthermore, we demonstrate the extraordinary sensing capability for single-TBN immunodetection theoretically, which will facilitate the studies of ultrasensitive biosensing and enable many new biosensing applications.

Appendix

A. The Explanation of Perturbation Theory

The 5 nm perturbation layer is always on the SiO_2, as shown in Fig. 6. As h_1 increases from 80 nm to 200 nm, $\Delta\lambda$ rises from 1.5 nm to 5.2 nm, and it decreases to 3.2 nm for h_1 changing from 200 nm to 230 nm. This indicates that the change of SiO_2 thickness inside the gold nanocylinders can lead to a significant spectral shift of the plasmonic resonance wavelengths.

B. TBN-Customized Plasmonic Metasensing

We add the simulation of 20 nm BE and 50 nm TBN, as shown in Fig. 7. We can optimize the height of SiO_2 nanocylinder and achieve the maximum TBN sensitivity of 6.34×10^{13} RIU^{-1}m^{-2} at the value of 130 nm. This is higher than that of the traditional PSPR sensing. The use of 130 nm hight SiO_2 nanocylinder in the M/D hybrid metasurface indicates the best TBN sensitivity, which is about 7 times of that for the traditional LSPR method.

References

[1] A. Prasad et al., "Nanohole array plasmonic biosensors: Emerging point-of-care applications," *Biosensors Bioelectron.*, vol. 130, pp. 185–203, Apr. 2019, doi: 10.1016/j.bios.2019.01.037.
[2] K.-L. Lee et al., "Nanoplasmonic biochips for rapid label-free detection of imidacloprid pesticides with a smartphone," *Biosensors Bioelectron.*, vol. 75, pp. 88–95, Jan. 2016, doi: 10.1016/j.bios.2015.08.010.
[3] J. Cai et al., "Solution-processed large-area gold nanocheckerboard metasurfaces on flexible plastics for plasmonic biomolecular sensing," *Adv. Opt. Mater.*, vol. 7, Jul. 2019, Art. no. 1900516, doi: 10.1002/adom.201900516.
[4] W. Li et al., "Aluminum nanopyramid array with tunable ultraviolet-visible-infrared wavelength plasmon resonances for rapid detection of carbohydrate antigen 199," *Biosensors Bioelectron.*, vol. 79, pp. 500–507, May 2016, doi: 10.1016/j.bios.2015.12.038.
[5] J. Zhu et al., "Low-cost flexible plasmonic nanobump metasurfaces for label-free sensing of serum tumor marker," *Biosensors Bioelectron.*, vol. 150, Feb. 2020, Art. no. 111905, doi: 10.1016/j.bios.2019.111905.
[6] J. Zhu et al., "Imprinted plasmonic measuring nanocylinders for nanoscale volumes of materials," *Nanophotonics*, vol. 9, pp. 167–176, Nov. 2019, doi: 10.1515/nanoph-2019-0369.
[7] L. K. Chin et al., "Plasmonic sensors for extracellular vesicle analysis: From scientific development to translational research," *ACS Nano*, vol. 14, no. 11, pp. 14528–14548, Oct. 2020, doi: 10.1021/acsnano.0c07581.
[8] J. Zhou et al., "Portable tumor biosensing of serum by plasmonic biochips in combination with nanoimprint and microfluidics," *Nanophotonics*, vol. 8, pp. 307–316, Jan. 2019, doi: 10.1515/nanoph-2018-0173.
[9] S. Kim et al., "Nonnoble-metal-based plasmonic nanomaterials: Recent advances and future perspectives," *Adv. Mater.*, vol. 30, no. 42, Mar. 2018, Art. no. 1704528, doi: 10.1002/adma.201704528.
[10] B. Špačková, P. Wrobel, M. Bocková, and J. Homola, "Optical biosensors based on plasmonic nanostructures: A review," *Proc. IEEE*, vol. 104, no. 12, pp. 2380–2408, Dec. 2016, doi: 10.1109/JPROC.2016.2624340.
[11] F. Li et al., "Exploring near-field sensing efficiency of complementary plasmonic metasurfaces for immunodetection of tumor markers," *Biosensors Bioelectron.*, vol. 203, May 2022, Art. no. 114038, doi: 10.1016/j.bios.2022.114038.
[12] F. Jiao et al., "Wafer-scale flexible plasmonic metasurface with passivated aluminum nanopillars for high-sensitivity immunosensors," *Sensors Actuators B*, vol. 344, Oct. 2021, Art. no. 130170, doi: 10.1016/j.snb.2021.130170.
[13] J. Nan et al., "Ultrahigh-sensitivity sandwiched plasmon ruler for label-free clinical diagnosis," *Adv. Mater.*, vol. 32, no. 2, Nov. 2020, Art. no. 1905927, doi: 10.1002/adma.201905927.
[14] L. Zhu et al., "Label-free quantitative detection of tumor-derived exosomes through surface plasmon resonance imaging," *Anal. Chem.*, vol. 86, no. 17, pp. 8857–8864, Aug. 2014, doi: 10.1021/ac5023056.
[15] E. Lee et al., "Size-dependent structural evolution of the biomineralized iron-core nanoparticles in ferritins," *Appl. Phys. Lett.*, vol. 102, no. 13, Apr. 2013, Art. no. 133703, doi: 10.1063/1.4801310.
[16] R. Saber et al., "High resolution imaging of IgG and IgM molecules by scanning tunneling microscopy in air condition," *Scientia Iranica*, vol. 18, no. 6, pp. 1643–1646, Dec. 2011, doi: 10.1016/j.scient.2011.11.028.
[17] Y. Tan et al., "A nanoengineering approach for investigation and regulation of protein immobilization," *ACS Nano*, vol. 2, no. 11, pp. 2374–2384, Oct. 2008, doi: 10.1021/nn800508f.
[18] N. H. L. Nguyen et al., "COVID-19 spike protein induced phononic modification in antibody-coupled graphene for viral detection application," *ACS Nano*, vol. 15, no. 7, pp. 11743–11752, Jun. 2021, doi: 10.1021/acsnano.1c02549.

[19] H. Im et al., "Label-free detection and molecular profiling of exosomes with a nano-plasmonic sensor," *Nature Biotechnol.*, vol. 32, no. 5, pp. 490–495, Apr. 2014, doi: 10.1038/nbt.2886.

[20] M. Gao et al., "Plasmonic resonance-linewidth shrinkage to boost biosensing," *Photon. Res.*, vol. 8, no. 7, pp. 1226–1235, 2020, doi: 10.1364/PRJ.390343.

[21] A. Belushkin, F. Yesilkoy, and H. Altug, "Nanoparticle-enhanced plasmonic biosensor for digital biomarker detection in a microarray," *ACS Nano*, vol. 12, no. 5, pp. 4453–4461, May 2018, doi: 10.1021/acsnano.8b00519.

[22] L. Huang et al., "One-step rapid quantification of SARS-CoV-2 virus particles via low-cost nanoplasmonic sensors in generic microplate reader and point-of-care device," *Biosensors Bioelectron.*, vol. 171, Jan. 2021, Art. no. 112685, doi: 10.1016/j.bios.2020.112685.

[23] J. Fan et al., "Plasmonic metasurfaces based on nanopin-cavity resonator for quantitative colorimetric ricin sensing," *Small*, vol. 13, no. 1, Oct. 2017, Art. no. 1601710, doi: 10.1002/smll.201601710.

[24] Y. Liang et al., "Large-scale plasmonic nanodisk structures for a high sensitivity biosensing platform fabricated by transfer nanoprinting," *Adv. Opt. Mater.*, vol. 7, no. 7, Feb. 2019, Art. no. 1801269, doi: 10.1002/adom.201801269.

[25] K. V. Sreekanth et al., "Extreme sensitivity biosensing platform based on hyperbolic metamaterials," *Nature Mater.*, vol. 15, pp. 621–627, 2016, doi: 10.1038/nmat4609.

[26] R. Yan et al., "Highly sensitive plasmonic nanorod hyperbolic metamaterial biosensor," *Photon. Res.*, vol. 10, no. 1, pp. 84–95, Jan. 2022, doi: 10.1364/PRJ.444490.

[27] D. Garoli et al., "Nanoporous gold metamaterials for high sensitivity plasmonic sensing," *Nanoscale Horiz.*, vol. 4, pp. 1153–1157, May 2019, doi: 10.1039/C9NH00168A.

[28] A. V. Kabashin et al., "Plasmonic nanorod metamaterials for biosensing," *Nature Mater.*, vol. 8, pp. 867–871, Oct. 2009, doi: 10.1038/nmat2546.

[29] Y. Liang et al., "Nanoprinted biosensors: Large-scale plasmonic nanodisk structures for a high sensitivity biosensing platform fabricated by transfer nanoprinting," *Adv. Opt. Mater.*, vol. 7, no. 7, Apr. 2019, Art. no. 1970026, doi: 10.1002/adom.201970026.

[30] J. Zhu et al., "Simultaneous fabrication of two kinds of plasmonic crystals by one nanoimprint mold," *IEEE Photon. Technol. Lett.*, vol. 29, no. 6, pp. 504–506, Mar. 2017, doi: 10.1109/LPT.2017.2649543.

[31] T. Xu et al., "Strategies to improve performances of LSPR biosensing: Structure, materials, and interface modification," *Biosensors Bioelectron.*, vol. 174, no. 4, Feb. 2020, Art. no. 112850, doi: 10.1016/j.bios.2020.112850.

[32] Y. Lee et al., "Low temperature atomic layer deposition of SiO_2 thin films using di-isopropylaminosilane and ozone," *Ceram. Int.*, vol. 43, no. 2, pp. 2095–2099, Feb. 2017, doi: 10.1016/j.ceramint.2016.10.186.

[33] Y. Wang et al., "An optofluidic metasurface for lateral flow-through detection of breast cancer biomarker," *Biosensors Bioelectron.*, vol. 107, pp. 224–229, Jun. 2018, doi: 10.1016/j.bios.2018.02.038.

[34] D. Harpaz et al., "Functionalized silicon dioxide self-referenced plasmonic chip as point-of-care biosensor for stroke biomarkers NT-proBNP and S100β," *Talanta*, vol. 212, May 2020, Art. no. 120792, doi: 10.1016/j.talanta.2020.120792.

[35] R. F. Harrington, *Time-Harmonic Electromagnetic Fields*. New York, NY, USA: McGraw-Hill, pp. 331–332, 1961.

[36] S. J. Zalyubovskiy et al., "Theoretical limit of localized surface plasmon resonance sensitivity to local refractive index change and its comparison to conventional surface plasmon resonance sensor," *J. Opt. Soc. Amer. A*, vol. 29, no. 6, Jun. 2012, Art. no. 994, doi: 10.1364/JOSAA.29.000994.

[37] O. Kedem et al., "Sensitivity and optimization of localized surface plasmon resonance transducers," *ACS Nano*, vol. 5, no. 2, pp. 748–760, Jan. 2011, doi: 10.1021/nn102617d.

[38] J. A. Jackman et al., "Plasmonic nanohole sensor for capturing single virus-like particles toward virucidal drug evaluation," *Small*, vol. 12, no. 9, pp. 1159–1166, Oct. 2016, doi: 10.1002/smll.201501914.

[39] R. Kalluri and V. S. LeBleu, "The biology, function, and biomedical applications of exosomes," *Science*, vol. 367, no. 6478, Feb. 2020, Art. no. eaau6977, doi: 10.1126/science.aau6977.

[40] O. Yavas et al., "On-a-chip biosensing based on all-dielectric nanoresonators," *Nano Lett.*, vol. 17, no. 7, pp. 4421–4426, Jun. 2017, doi: 10.1021/acs.nanolett.7b01518.

[41] X. Hadoux et al., "Non-invasive in vivo hyperspectral imaging of the retina for potential biomarker use in Alzheimer's disease," *Nature Commun.*, vol. 10, Sep. 2019, Art. no. 4227, doi: 10.1038/s41467-019-12242-1.

[42] AVS-RACKMOUNT-USB2, Avantes BV, Netherlands. [Online]. Available: https://www.avantes.com/

Jiaqing Shen was born in Henan, China. She received the B.S. degree from the Henan University of Science and Technology, Luoyang, China, in 2019. She is currently working toward the Ph.D. degree with Xiamen University, Xiamen, China. Her research interests include metasurface, biophotonics, and biosensing applications.

Fajun Li received the B.S. degree from the Nanjing University of Science and Technology Zijin College, Nanjing, China, in 2019. Since September 2020, he has been working toward the Ph.D. degree with Xiamen University, Xiamen, China. His research interests include nanophotonics, nanofabrication, plasmonics, metasurface, and lable-free biosensors.

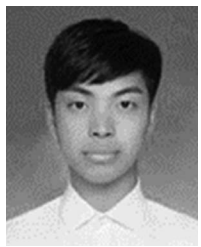

Zhenbiao Wang was born in Bozhou, Anhui, China. He is currently studying with Xiamen University, Xiamen, China, majoring in electronic information. He has authored or coauthored a paper in the international journal *Sensors*, as the first author in 2021. His research focuses on plasmonic metasurface biosensing.

Xueying Liu was born in Henan, China, in 1995. She received the B.S. and M.S. degrees in 2017 and 2019, respectively. She is currently working toward the Ph.D. degree with Xiamen University, Xiamen, China. Her research interests include terahertz metamaterials and sensing applications.

Yinong Xie was born in Zhangzhou, Fujian, China, in 1995. He received the B.S. and M.S. degrees from the Qingdao University of technology, Qingdao, China, in 2017 and 2020, respectively. He is currently working toward the Ph.D. degree with Xiamen University, Xiamen, China. His research interests include terahertz sensing, biosensing, metasurfaces, and the interaction of matter and electromagnetic wave.

Wei Chen was born in Taizhou, Jiangsu, China. He received the B.S. degree from Changzhou University, Changzhou, China, in 2018, and the M.S. degree from Jimei University, Xiamen, China, in 2021. He is currently working toward the Ph.D. degree with Xiamen University, Xiamen. His research interests include the interaction of matter and light, including metasurface, bound states in the continuum, and inverse design. He was a Reviewer of many academic journals, including *2D materials*, *Optics Express*, *Journal of Optics*, and *Journal of Physics: Condensed Matter*.

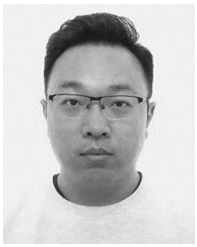

Ming Hui Fang was born in Taichung, Taiwan. He received the M.S. degree in mechanical engineering from the National Taiwan University of Science and Technology, New Taipei, Taiwan, in 2009. He is currently working toward the Ph.D. degree with Xiamen University, Xiamen, China. He is currently with Quanzhou Sanan Integrated Circuit Company, Ltd. He is a major on crystal technology, CMP technology and wafer bonding technology. His research interests include metamaterials, biosensors, and SAW sensor.

Jinfeng Zhu (Senior Member, IEEE) received the B.S. degree in electronic communication science and technology and the Ph.D. degree in physical electronics from the University of Electronic Sci ence and Technology of China, Chengdu, China, in 2006 and 2012, respectively. From November 2009 to November 2011, he was a Visiting Researcher with the Device Research Laboratory and Department of Electrical Engineering, University of California, Los Ange les, CA, USA. From July 2017 to 2018, he was a Visiting Professor with the Optoelectronics Research Centre, University of Southampton, Hampshire, U.K. Since July 2012, he has been with Xiamen University, Xiamen, China, where he is currently the Associate Dean and Professor in the Institute of Electromagnetics and Acoustics. He is the Fellow of International Association of Advanced Materials, and serves as the Associate Editor of Frontiers in Materials. His research interests include nanophotonics, plasmonics, metamaterials, van der Waals materials, and related sensing applications.